Received: 17 September 2021 | Revised: 29 July 2022 | Accepted: 24 November 2022

DOI: 10.1002/met.2123

Meteorological Applications
Science and Technology for Weather and Climate
Open Access
RMetS

RESEARCH ARTICLE

Effects of COVID-19 lockdown measures on nitrogen dioxide and black carbon concentrations close to a major Italian motorway

Elena Bertazza[1] | **Andrea Bisignano**[1,2] | **Marco Falocchi**[3] | **Lorenzo Giovannini**[1]

[1]Department of Civil, Environmental and Mechanical Engineering, University of Trento, Trento, Italy

[2]Environmental Protection Agency of the Liguria Region, Air Quality Unit, Genoa, Italy

[3]CISMA s.r.l., Centro di Ingegneria e Sviluppo Modelli per l'Ambiente, Bolzano, Italy

Correspondence
Lorenzo Giovannini, Atmospheric Physics Group, Department of Civil, Environmental and Mechanical Engineering, University of Trento, Via Mesiano, 77, Trento I-38123, Italy.
Email: lorenzo.giovannini@unitn.it

Funding information
European Commission, BrennerLEC project, Grant/Award Number: LIFE15 ENV/IT/000281

Abstract

During the first half of 2020, the Italian government imposed several restrictions to limit the spread of the COVID-19 pandemic: at the beginning of March, a heavy lockdown regime was introduced leading to a drastic reduction of traffic and, consequently, traffic-related emissions. The aim of this study is to evaluate the effects of these restrictions on pollutant concentrations close to a stretch of the Italian A22 motorway lying in the Alpine Adige valley. In particular, the analysis focuses on measured concentrations of nitrogen dioxide (NO_2) and black carbon (BC). Results show that, close to the motorway, NO_2 concentrations dropped by around 45% during the lockdown period with respect to the same time period of the previous 3 years. The equivalent analysis for BC shows that the component related to biomass burning, mostly due to domestic heating, was not particularly affected by the restrictions, while the BC component related to fossil fuels, directly connected to traffic, plummeted by almost 60% with respect to the previous years. Since atmospheric concentrations of pollutants depend both on emissions and meteorological conditions, which can mask the variations in the emission regime, a random forest algorithm is also applied to the measured concentrations, in order to better evaluate the effects of the restrictions on emissions. This procedure allows for obtaining business-as-usual and meteorologically normalized time series of both NO_2 and BC concentrations. The results derived from the random forest algorithm clearly confirm the drop in NO_2 emissions at the beginning of the lockdown period, followed by a slow and partial recovery in the following months. They also confirm that, during the lockdown, emissions of the BC component due to biomass burning were not significantly affected, while those of the BC component related to fossil fuels underwent an abrupt drop.

KEYWORDS

black carbon, COVID-19, meteorological normalization, nitrogen dioxide, random forest, traffic-related pollution

1 | INTRODUCTION

In order to prevent the spread of the COVID-19 disease, during the first half of 2020 severe lockdown measures were taken all over the world. These measures caused a sudden halt in socio-economic human activities: many industrial sectors shut down and personal mobility was heavily restricted. The impact on traffic was huge: as the production activities stopped, the number of circulating heavy-duty vehicles drastically decreased and the restrictions on people's movement caused a sudden drop in the number of circulating light vehicles as well. Hence, as the traffic was reduced, the transport-related emissions immediately diminished too. Guevara et al., 2021 estimated that road transport was the main contributor to emission reduction in Europe during the COVID-19 lockdown period in 2020.

Vehicular traffic is responsible for the emission of different pollutants, among which carbon monoxide (CO), volatile organic compounds (VOCs), polycyclic aromatic hydrocarbons (PAHs), nitrogen monoxide (NO) and dioxide (NO_2) (sometimes collectively referred to as NO_x), and particulate matter (PM), which comprises black carbon (BC). In the present work, the attention focuses on the effects of the lockdown measures against COVID-19 on the emissions and atmospheric concentrations of two of these pollutants: NO_2 and BC. NO_2 represents nowadays one of the most problematic pollutants emitted by vehicles, with concentrations frequently exceeding the annual limit value of 40 $\mu g\, m^{-3}$, set by the European directive 2008/50/EU, alongside major roads. Exposure to high NO_2 concentrations can cause severe airway inflammation and increases the probability of cells being damaged by airborne viruses; it also has effects on blood cells (Frampton et al., 2002). On the other hand, BC is a component of PM2.5 and consists of fine carbonaceous particles produced by the incomplete combustion of fossil fuels and biomass. BC measurements allow for discerning between the component produced by biomass burning and the one emitted by the combustion of fossil fuels (Sandradewi et al., 2008). Although there are still no regulatory limits for BC concentrations, this pollutant is very harmful to human health as, when introduced into the body, causes cardiovascular and pulmonary diseases and might also lead to lung cancer (Laeremans et al., 2018; Magalhaes et al., 2018; Stabile et al., 2018).

Different studies have analysed the impact of COVID-19 lockdown measures on pollutant emissions and concentrations, highlighting different behaviours depending on the pollutant and the local context (e.g., Grange et al., 2021). NO_2 has generally been reported as one of the pollutants most impacted by lockdown measures, especially at traffic sites. For example, Sokhi et al., 2021 reported the results of a study coordinated by the World Meteorological Organization Global Atmospheric Watch (WMO/GAW), highlighting, from the analysis of data from 540 worldwide air quality stations, a clear correlation between the reduction in NO_2 concentrations and the reduction in people's mobility. Focusing on Europe, Solberg et al., 2021 found NO_2 concentration reductions of $\sim$ 60% in April 2020 in Spain, Italy, Portugal and France at traffic sites. On the other hand, the studies analysing the impact of lockdown measures on BC concentrations show more variable results, depending on the context and on the fraction of BC considered. For example, Liu et al., 2021 found a 20% increase in BC concentrations in Beijing during the lockdown period, contrasting a 70% decrease in Tibet. Goel et al., 2021 analysed BC contributions in Dehli during pre-lockdown and lockdown periods, highlighting a strong decrease in the component due to fossil fuels, while the component due to biomass burning experienced lower variations. The effect of lockdown measures on BC is generally clearer when considering data from traffic sites, as highlighted by Hudda et al., 2020, who analysed BC concentrations in an urban neighbourhood in Sommerville (Massachusetts), recording a concentration reduction of 22%–56% depending on the road class.

The analysis presented in this work focuses on pollutant concentrations measured along a stretch of the A22 Italian motorway (which is also called the Brenner motorway) entirely lying in the Adige valley, a glacial valley located in the northeastern Italian Alps. In this motorway stretch, meteorological conditions and pollutant concentrations are exceptionally well monitored in the framework of the European LIFE project Brenner-LEC, where LEC stands for "Lower Emissions Corridor". The project started in 2016 aiming at testing policies to reduce traffic-related pollution along the motorway, since in a fragile Alpine context high pollutant concentrations can be dangerous not only for people but also for wildlife and vegetation (Felzer et al., 2007). The monitoring network installed for this project allows for a comprehensive evaluation of the effects of the lockdown measures on pollutant concentrations not only close to the motorway, thus in positions directly affected by traffic-related emissions, but also at different distances from the road, thus also evaluating the effects of lockdown measures on background concentrations in an Alpine valley (Bisignano et al., 2022).

It is well known that pollutant concentrations measured by air quality stations depend not only on emissions, but also on meteorological conditions, and in particular on atmospheric dispersion. As a consequence, in the analysis of concentration measurements, changes in emission patterns can be at least partly masked by the meteorological

variability, and in particular by the alternation of periods more or less favourable for pollutant dispersion (Anh et al., 1997). Therefore, in order to gather information on the intrinsic emissions, one should be able to separate the two contributions. This is particularly important over complex terrain, where dispersion processes are usually much more complicated than over flat areas, as they are affected by a large range of atmospheric phenomena at different spatial scales (Giovannini et al., 2020). For example, mountain valleys, due to orographic shadowing and the convergence of katabatic winds from the slopes, are frequently influenced by stable stratification, with strong and persistent ground-based temperature inversions, which lead to reduced dispersion and pollutant accumulation in the lowest atmospheric layers (Clements et al., 2003; Neff & King, 1989; Quimbayo-Duarte et al., 2019). The most unfavourable conditions for pollutant dispersion occur during wintertime, when the weak solar radiation may fail to completely break up the nocturnal stable stratification, creating a shallow mixed layer topped by an elevated inversion, that traps pollutants close to the ground. These conditions can last for several days, causing severe air pollution episodes (de Franceschi & Zardi, 2009). Moreover, under fair weather conditions, temperature contrasts at different spatial scales cause the development of thermally-driven winds, which can play an important role in dispersion. In particular, daytime hours are characterized by up-slope and up-valley circulations, that transport pollutants from the plain and the bottom of the valley to higher altitudes, while down-slope and down-valley winds develop during nighttime (Zardi & Whiteman, 2013). Even in the case of strong synoptic forcing, the consequences for the dispersion can be different from valleys to plains. In fact, over plains, strong winds sweep away pollutants, while in a valley the penetration of the wind depends on the orientation of the valley axis with respect to the wind field, and on the depth of the valley itself, as high mountains and/or pre-existent stable layers obstacle wind intrusions (Mayr & Armi, 2010; Whiteman & Doran, 1993).

It is then clear that, especially over complex terrain, it is crucial, in order to evaluate changes in the emissions, to take into account the effects induced by meteorological conditions on local pollutant concentrations. This operation can be performed using a meteorological normalization procedure. This technique allows for discriminating the contribution of the emission sources from the effects of meteorological conditions on the variability of the observed concentration levels. In meteorological normalization procedures, the dependence of the measured concentration on different independent variables representative of both dispersion processes (e.g., meteorological variables) and emission variations (e.g., temporal variables) is evaluated, in order to eliminate the effects of atmospheric conditions on the measured concentrations, leaving only the intrinsic variations due to the emissions. In this way, a normalized time series showing a trend of concentrations independent from meteorological conditions can be obtained. Early meteorological normalization techniques involved the use of least square regressions (Deolal et al., 2012; Henneman et al., 2015; Lu & Chang, 2005; Sloane, 1984). This method has the disadvantage to be parametric, that is, it requires the introduction of some kind of explicit functional dependence, which can be challenging, given the complexity of processes in the atmospheric boundary layer. In recent times new non-parametric approaches have been developed, that is, machine learning algorithms that exploit large datasets to "understand" the complex relationship between the concentration and the independent variables. Hence, machine learning algorithms are statistical predictive methods that can be used to (a) make predictions of pollutant concentrations, knowing the meteorological data and making assumptions on the source emissions (b) produce a normalized time series, highlighting the variations in the intrinsic emissions. In this study, both these capabilities of the machine learning technique are exploited to better understand the effects of the COVID-19 restrictions on pollutant concentrations. The machine learning procedure here employed makes use of the *rmweather* R package (Grange et al., 2018; Grange & Carslaw, 2019), which is based on a random forest algorithm (details in Section 4). The same package was successfully used in several other studies aiming at discriminating the effects of changes in emissions from the meteorological variability (e.g., Falocchi et al., 2021; Mallet, 2020; Vu et al., 2019; Walker et al., 2019). In particular, Falocchi et al., 2021 analysed with this methodology multi-year NO_2 time series from different air quality stations located in a stretch of the Adige Valley slightly northward with respect to the area considered here. The same methodology was recently adopted also to evaluate the effects of COVID-19 on pollutant emissions by Grange et al., 2021, who compared observed and business-as-usual predicted concentrations in several European cities, and by Fenech et al., 2021, who applied this technique to pollutant concentrations measured in Malta. Grange et al., 2021, analysing data from 246 air quality stations located in 102 urban areas, found decreases in NO_2 concentrations of 34% and 32% at traffic and urban background stations respectively. Fenech et al., 2021 also highlighted a more significant decrease in NO_2 concentrations (54%) at a traffic site with respect to background stations.

The present paper is organized as follows: Section 2 illustrates the target area, Section 3 describes the datasets

used, while Section 4 briefly explains the random forest algorithm. The analysis of the measured concentrations of NO_2 and BC is presented in Section 5, along with the results obtained with the machine learning algorithm. Finally, conclusions are drawn in Section 6.

2 | STUDY AREA

The A22 motorway starts from the border with Austria, at the Brenner Pass, flows along the Isarco and Adige valleys in the Italian Alps, and ends close to the town of Modena, in the Po Plain. It is an important infrastructure connecting Italy to Central Europe, and, in particular, it is the busiest Alpine corridor, moving approximately 40,000 vehicles per day, with higher peaks during holidays. The motorway stretch considered here is entirely located within the southern Adige valley, where both rural areas and urban settlements can be found (Figure 1). The floor of the Adige valley is approximately 2 km wide, and it is flanked by peaks reaching heights of 1500–2000 m above the valley floor.

In the present study, data from six air quality stations located at different distances from the A22 motorway are analysed (Figure 1). Three of them (BL103, BL107 and BL164) are located close to the motorway, at a distance of about 10 m from the traffic centreline. This positioning allows for the direct measurement of traffic-induced pollution and, for this reason, as stated by the European directive 2008/50/CE, these stations are classified as traffic stations. Avio is located 16 m from the motorway centreline and thus it is still representative of traffic-related emissions. The other two stations (Cortina and Mezzolombardo), from now on referred to as rural stations, are located respectively at 230 and 800 m from the motorway, far from major pollutant sources, and their

FIGURE 1 Map of the Adige Valley. The black line indicates the A22 motorway, with the red part being the stretch between San Michele all'Adige and Egna considered in Section 3.4 for the analysis of traffic data. The red dots indicate the reference meteorological and air quality stations, while the blue dots refer to the weather stations used for the calculation of the lapse rate. The aeroplane shows the position of the temperature profiler at the Bolzano airport and the green squares indicate the largest urban centres of the area. Background map from Google Earth.

observations will be used to assess the effect of lockdown measures on background pollutant levels in the rural areas of the valley floor. In particular, the analysis of measurements from air quality stations located in different local contexts allows for the investigation of the impact of lockdown measures at different distances from the motorway. The details regarding the position and the instruments installed in these six stations are listed, respectively, in Tables 1 and 2. Both the instruments measuring NO_2 concentrations have an accuracy of ±1% full-scale, while the aethalometer that provides BC measurements has a resolution of 1 ng m^{-3} and a sensitivity of 0.03 μg m^{-3}.

3 | DATASET AND TEMPORAL VARIABLES

In this section, the dataset used in the present study is presented, including the air quality measurements, the independent variables adopted in the random forest procedure and the traffic data. In particular, the independent variables can be divided into meteorological and temporal variables, which are representative of the dispersion processes and of the periodical emission variations respectively. It is important to include all the variables that can have an influence on concentrations, otherwise, the random forest algorithm may not be able to correctly predict observed concentrations and the normalized trends might show a residual variability not caused by changes in the emission regime. On the contrary, if an irrelevant variable is used, the algorithm will simply ignore it (Ziegler & König, 2014). The dataset analysed covers the time period from 1 January 2017 to 20 July 2020, in order to compare air quality conditions along the motorway between periods with normal traffic flows and periods affected by the lockdown measures. Air quality, meteorological and traffic measurements adopted in this study were provided as 10-min data, which were then aggregated to daily averages for the following analyses, except for precipitation and traffic, which were summed in order to obtain daily cumulative values.

3.1 | Concentrations

3.1.1 | NO_2

The NO_2 concentration series provided by the air quality stations were controlled for data quality and cleaned by removing the outliers. The outliers removal was performed by calculating the logarithm of the single measurements and excluding the measurements lying outside the 3σ intervals evaluated on a daily basis. The original distribution was, in fact, skewed towards low values and using this rule on the untransformed data would have excluded only the outliers on the high end of the distribution, while leaving unaffected unrealistically low concentration values. The percentage of excluded data among the datasets of the various stations ranges between 0.6% and 1.5%. This low percentage ensures that the data quality procedure is appropriate and that only unrealistically high and low concentration values were removed. Data were finally aggregated at daily frequency, calculating the average concentration and excluding days with data availability less than 75%.

3.1.2 | Black carbon

Black carbon measurements were performed, at the two traffic stations BL103 and BL164, with the Maegee Scientific aethalometer AE33, exploiting the capacity of BC particles to absorb and scatter light. Inside the instrument, the aerosol is illuminated by radiation, and then the absorption coefficient is evaluated and converted into a concentration value. The absorption is measured at 7 wavelengths simultaneously: 370, 470, 520, 590,

TABLE 1 Position, altitude, pollutants measured and distance from the motorway centreline of the air quality stations analysed in this work.

Station	Position	Altitude (m a.s.l.)	Pollutants	Motorway distance (m)
BL103	46.32° N 11.27° E	230	NO_2, BC	10
BL107	46.29° N 11.24° E	220	NO_2	10
BL164	45.87° N 11.0° E	190	NO_2, BC	10
Avio	45.74° N 10.97° E	139	NO_2	16
Cortina	46.27° N 11.23° E	210	NO_2	230
Mezzolombardo	46.2° N 11.11° E	227	NO_2	800

TABLE 2 Instruments installed at the air quality stations analysed in this work.

Station	Parameter	Model
BL103	Meteo	SIAP+MICROS sensors
	NO_2	Horiba APNA 370
	BC	Magee scientific Aethalometer AE33
BL107	Meteo	SIAP+MICROS sensors
	NO_2	Horiba APNA 370
BL164	Meteo	Davis—Vantage Pro2
	NO_2	Horiba APNA 370
	BC	Magee scientific Aethalometer AE33
Avio	Meteo	Davis—Vantage Pro2
	NO_2	Thermo 42i
Cortina	Meteo	SIAP+MICROS sensors
	NO_2	Horiba APNA 370
Mezzolombardo	Meteo	Davis—Vantage Pro2
	NO_2	Thermo 42i

660, 880 and 950 nm and the total BC concentration is directly derived from the 880 nm absorption coefficient, b (880). In this study, the BC component produced by fossil fuel combustion (BC_{ff}), mainly related to traffic, and the one caused by biomass burning (BC_{bb}), mainly related to domestic heating, are analysed. These components have been derived following Sandradewi et al., 2008. In particular, it was assumed that the absorption coefficients of the two components have the following wavelength dependence: λ^{-1} for BC_{ff} and λ^{-2} for BC_{bb}, and measurements at 470 and 950 nm were used to calculate the fraction of each component. The BC outliers were removed by adopting the same technique used for NO_2 concentrations; in this case, the percentage of removed data is 0.6%. The concentrations of the two components, BC_{ff} and BC_{bb}, were found by multiplying the total BC concentration by the respective fractions. Finally, for both BC_{ff} and BC_{bb} time series, data were aggregated at daily frequency using the same methods adopted for NO_2.

3.2 | Meteorological variables

The near-surface meteorological measurements used to feed the random forest procedure implemented were provided by the air quality stations themselves. In particular, the near-surface meteorological quantities selected as independent variables are temperature, pressure, relative humidity, global solar radiation (global solar radiation

TABLE 3 Position and altitude of the meteorological stations used for the lapse rate calculation.

Station	Position	Altitude (m a.s.l.)
Brentonico	45.82° N 10.96° E	727
Malga Zugna	45.81° N 11.06° E	1620
Faedo	46.19° N 11.17° E	696
Cima Paganella	46.14° N 11.04° E	2125

data at Cortina presented long gaps, which were filled using radiation measurements performed at BL107, given the closeness of the two stations), precipitation, wind speed and wind direction. Since atmospheric stability is an important parameter influencing atmospheric dispersion, the temperature lapse rate is also taken into account. For BL103, BL107 and Cortina, located in the northern part of the study area, the values of the temperature lapse rate were derived from the data of the temperature profiler located at the airport of the city of Bolzano (Figure 1). This instrument provides temperature measurements up to 1000 m above ground level (AGL), with a spatial resolution of 50 m. The data of the 21 vertical levels provided by the temperature profiler were also in this case aggregated in order to get the average daily temperature for each level. Then, for every day, two different lapse rates were calculated from a linear regression on the data of the lowest 100 and 500 m AGL respectively. On the other hand, Mezzolombardo, BL164 and Avio are located far away from the temperature profiler, so the lapse rate values obtained from its measurements might not be representative of their local conditions. Therefore, for these stations, the lapse rate was also calculated from the difference between the temperature measured by the air quality station and that measured by another weather station located in the same area but at a higher altitude. In particular, Cima Paganella and Faedo were used to calculate the lapse rate for the normalization of air quality data at Mezzolombardo, while Brentonico and Malga Zugna were adopted for the normalization procedure at BL164 and Avio. Their position, along with the location of the temperature profiler, are indicated in Figure 1 and their details are reported in Table 3.

3.3 | Temporal variables

Some temporal variables are introduced as independent variables in the random forest algorithm in order to describe periodical changes in pollutant emissions caused by, for example, variations in traffic or domestic heating. In particular, the variables here considered are the Julian day, the weekday and the Unix date. The Julian day

indicates the day number of the year, it is a value ranging from 1 to 365 (or 366) and it helps to describe the seasonal cycles of pollutant concentrations. For example, for both NO_2 and BC, concentrations are expected to be higher on days with a Julian day value close to 1 or 365 (winter days). The weekday, instead, indicates the day number of the week, it goes from 1 to 7 and describes weekly cycles. For example, on Sundays (weekday = 7) concentrations close to the motorway are expected to decrease with respect to the other days of the week, because of the prohibition of circulation of heavy vehicles. Finally, the Unix date (number of seconds since 1970-01-01) is the trend term and is introduced to describe the long–term fluctuations of concentrations, for example, declining trends due to the car fleet renewal, and those variations amenable to other explanatory variables not taken into account. Hence, the concentration partial dependence on the Unix date shows the concentration trend deprived of the effects of the other independent variables, which is basically the behaviour of the normalized series.

3.4 | Traffic variables

The number of vehicles transited on the motorway stretch between San Michele all'Adige and Egna (red stretch in Figure 1) was provided by measurements performed with an inductive loop. These data allow the quantitative evaluation of the effect of COVID-19 restrictions on motorway traffic, as can be appreciated in Figure 2, which shows the time series of the number of vehicles (light, heavy and total) in the period from January to July in 2020 and in the years 2017–2019. The background colours in Figure 2 evidence four time periods, characterized by different traffic conditions, that are defined according to the changes in the restrictions imposed by the Italian government:

- 1 January–24 February (unaltered period): no restrictions were in place. The comparison between the average daily number of transiting vehicles during this period in 2020 and over the same time period in the three previous years (2017–2019) evidences that in 2020 the number of both light and heavy vehicles increased, respectively, by 9% and 4%.
- 25 February–8 March (transition period): in this period restrictions were introduced only in areas where infected people were found. During this phase in 2020 the number of light vehicles diminished by 16%, while heavy traffic increased by 4% with respect to the three previous years.
- 9 March–2 June (lockdown): during this period heavy restrictions were in place in the country; in 2020 the traffic along the A22 motorway decreased by 38% for heavy-duty vehicles and by 85% for light vehicles with respect to the three previous years.
- 3 June–20 July (upturn): the possibility to move between regions was restored and the borders with

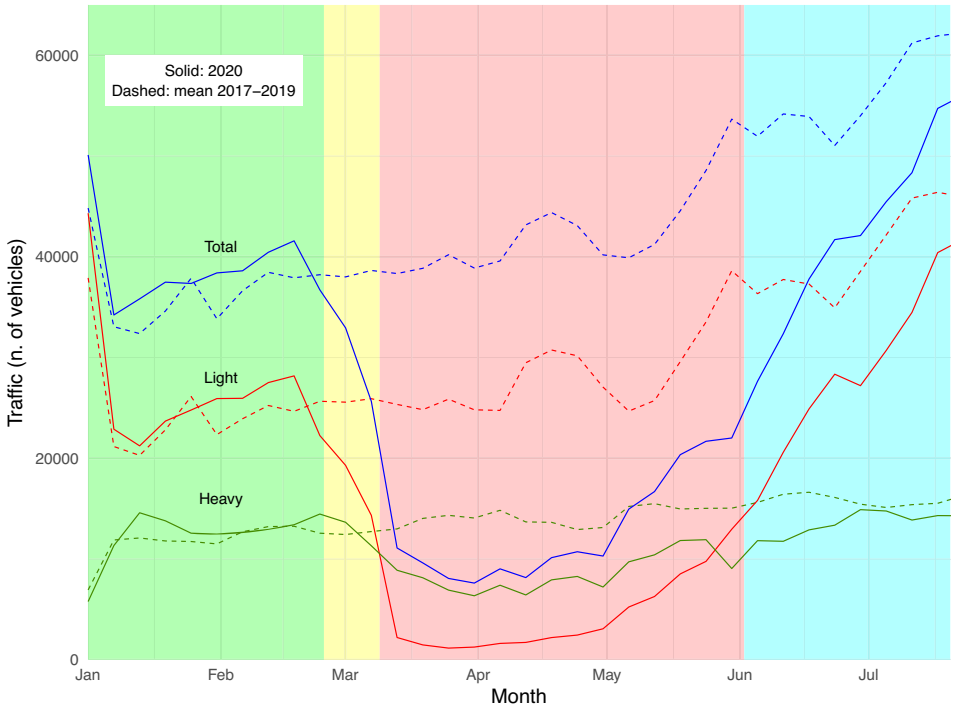

FIGURE 2 Time series of the daily number of transiting vehicles on the San Michele all'Adige-Egna motorway stretch. The plot shows weekly means, solid lines indicate 2020 values, while dashed lines 2017–2019 average values. Colours are used to distinguish between vehicle types: light vehicles (red), heavy vehicles (green) and total (light+heavy vehicles, blue). Background colours indicate the different periods individuated: unaltered (green), transition (yellow), lockdown (red) and upturn (cyan).

Austria and Germany were re-opened. With the lightening of the restrictions, in 2020 the traffic increased but still did not reach the levels of the three previous years, showing a diminution for both light and heavy vehicles of 30% and 16% respectively. During this period the light vehicle traffic shows a progressive increase also in 2017–2019, due to the touristic flow related to summer holidays.

These periods are taken as a reference in the analyses presented in the following parts of the paper, in particular for the comparison between pollutant concentrations observed in 2020 and in the three previous years.

4 | RANDOM FOREST PROCEDURE

The predictive and meteorologically normalized time series are obtained by exploiting the *rmweather* R package (Grange et al., 2018; Grange & Carslaw, 2019), a random forest code that uses the machine learning decision tree technique for training and predictions. A decision tree algorithm is a regression method based on binary splits: observations are recursively divided into two different groups generated using some intervals of values of the independent variables. The process continues until all groups consist of a single element or elements of the same class (Ho, 1995). The number of splits can also be limited by introducing more specific stopping rules, for example, a minimum number of elements per group can be set in order to prevent further splitting. Another method consists in growing a full tree and then removing the splits that provide less information, this technique is called "pruning". A lower number of splits allows the decision trees to be not too complex or too dependent on the input data (Song & Ying, 2015). This whole process is called training and the classification rules obtained from the initial data can then be used to describe some new data and make predictions. However, a single decision tree can be very complex and, while it can perfectly describe the input data, it often fails to interpret data that were not used in the training process (Kotsiantis, 2013). This issue is called overfitting and it is solved using a random forest algorithm, a code that grows multiple decision trees and combines their predictions into a single prediction that is more accurate than the ones obtained with a single decision tree. This random forest model also allows for determining the influence of each independent variable on the dependent one. The procedure used in this study is described in the following:

1. *Dataset spitting*: the input dataset consists of time series indicating, for every day, the correspondent values of pollutant concentration, meteorological and time variables. This dataset is divided into two smaller sets: the training and the testing sets. In particular, 80% of the days are used for training and the other 20% for testing.
2. *Tree growing*: 300 decision trees, having at least 5 nodes, are produced using 300 different growth datasets derived from the training set. Each growth dataset is obtained using the bootstrap aggregation technique (Breiman, 1996): the days are randomly sampled with replacement from the training set and the independent variables are sampled too. Each growth dataset has the same number of observations of the training set, but a smaller number of independent variables. The fact that the number of observations used is the same as the training set does not mean that all the observations are used for each tree since, because of the sampling with replacement, some are not selected and some are selected multiple times. The number of independent variables in the growth datasets is set equal to the rounded value of the square root of the total number of independent variables, following Grange & Carslaw, 2019 and Falocchi et al., 2021. The random sampling of both the dataset and the independent variables allows the trees to be decorrelated from one another, as they are grown using both different data and variables. This group of trees constitutes the random forest and its predictions are obtained by combining via arithmetic mean the predictions of the single trees.
3. *Random forest testing*: the part of the input dataset (20% in this case) not used for training is called Out-of-Bag data and it is employed for testing the random forest output. The model is used to predict the concentration values from the independent variables, then the predicted values are compared to the real ones. The R^2 coefficient and the root mean square error (RMSE) are calculated to assess the accuracy of the model.
4. *Predictions*: the trained random forest model can be used to predict pollutant concentrations. For this purpose, in this work the model is trained using data in the time interval 2017–2019, while concentrations are predicted for 2020. In this way, the model is expected to predict a business-as-usual scenario, that is, the concentrations that would have been measured without the restrictions introduced by the lockdown. Therefore, the differences between predicted and observed concentrations can be interpreted, neglecting the possible errors introduced by the statistical procedure used, such as the effects of the COVID-19 pandemic on pollutant concentrations. This comparison is presented and commented on in Section 5.2.

5. *Normalization*: the normalized time series are produced using the predictions of the random forest model, trained over the entire time interval 2017–2020. For each point of the series, all the independent variables, except the Unix date, are sampled without replacement from the input dataset 1000 times. These samples, hence, have the same Unix date (the one of that particular day), but each of them presents 1000 different values for the other independent variables. The random forest model is used on all the samples, obtaining 1000 different predictions. These predictions are aggregated using a mean in order to get a single concentration value: the normalized value for that day. The complete normalized series is obtained by repeating this procedure for all the days of the dataset. Since the Unix date is kept fixed, while the contributions to the concentration caused by all the other independent variables are averaged, the normalized trend follows the partial dependence trend relative to the Unix date. Finally, since the results of a single random forest model depend on the initial choice of the training/testing sets, 20 different models are produced using an iterative process that repeats steps 1–3 and 5 for 20 times. The final results are then obtained as the average of the output of the 20 models. This also allows for evaluating uncertainty, which would have been impossible to determine using only one model. The normalized time series are presented in Section 5.3.

5 | RESULTS

5.1 | Observed concentrations

5.1.1 | NO_2

The calendar plots reported in Figure S1 show NO_2 daily concentrations measured during the periods January-July 2019 and January-July 2020 at BL107, with the colour scale indicating the concentration values. It is already clear from this first analysis that, starting from March, NO_2 concentrations were considerably lower in 2020 than in 2019, highlighting the effects of the strong decrease in traffic emissions during the lockdown period.

Table 4 shows the comparison between the average values of the measured NO_2 and BC concentrations in 2020 and in 2017–2019 in the periods from 1 January to 24 February (unaltered) and from 9 March to 2 June (lockdown). The first period was taken into account to evaluate possible changes in concentrations not related to the restrictions, hence allowing for a better contextualization of the decrease caused by the lockdown. Table 4 indicates that, for each station, during this period the average NO_2 concentration was similar to that registered during the three previous years. On the other hand, in the lockdown period, a significant decrease at all the air quality stations was detected, ranging between 38% and

TABLE 4 Comparison between NO_2 and BC mean concentration values for all the stations in the unaltered and lockdown periods.

NO_2	Unaltered (1 January–24 February)	Lockdown (9 March–2 June)
BL103		
Mean 2017–2019 [μg m^{-3}]	67.7	51.2
Mean 2020 [μg m^{-3}]	67.6	26.7
Percentage change	−0.2%	−47.8%
BL107		
Mean 2017–2019 [μg m^{-3}]	69.7	48.2
Mean 2020 [μg m^{-3}]	67.5	25.3
Percentage change	−3.1%	−47.6%
BL164		
Mean 2017–2019 [μg m^{-3}]	74.3	54.6
Mean 2020 [μg m^{-3}]	76.5	30.6
Percentage change	+3.1%	−43.9%
Avio		
Mean 2017–2019 [μg m^{-3}]	64.7	44.7
Mean 2020 [μg m^{-3}]	58.8	24.6
Percentage change	−9.0%	−44.9%
Mezzolombardo		
Mean 2017–2019 [μg m^{-3}]	34.8	18.0
Mean 2020 [μg m^{-3}]	35.6	11.2
Percentage change	+2.4%	−38.0%
Cortina		
Mean 2017–2019 [μg m^{-3}]	46.6	23.3
Mean 2020 [μg m^{-3}]	47.0	13.6
Percentage change	+1.0%	−41.6%
BC	**Unaltered (1 January–24 February)**	**Lockdown (9 March–2 June)**
BL164 BC_{ff}		
Mean 2017–2019 [ng m^{-3}]	3291	2102
Mean 2020 [ng m^{-3}]	3469	883
Percentage change	+5.4%	−58.0%
BL164 BC_{bb}		
Mean 2017–2019 [ng m^{-3}]	957	255
Mean 2020 [ng m^{-3}]	1061	218
Percentage change	+10.8%	−14.6%

48%. As expected, the traffic stations show a larger percentage decrease than the rural ones, since they are more influenced by traffic conditions. For the same reason, between the two rural stations, the one exhibiting the larger percentage diminution is Cortina, which is closer to the motorway than Mezzolombardo (see Table 1). Figure 3 shows the time series of NO_2 concentrations measured at all the air quality stations in the time span of 2017–2020. In order to make the graphics clearer, weekly average values are here reported. Being located

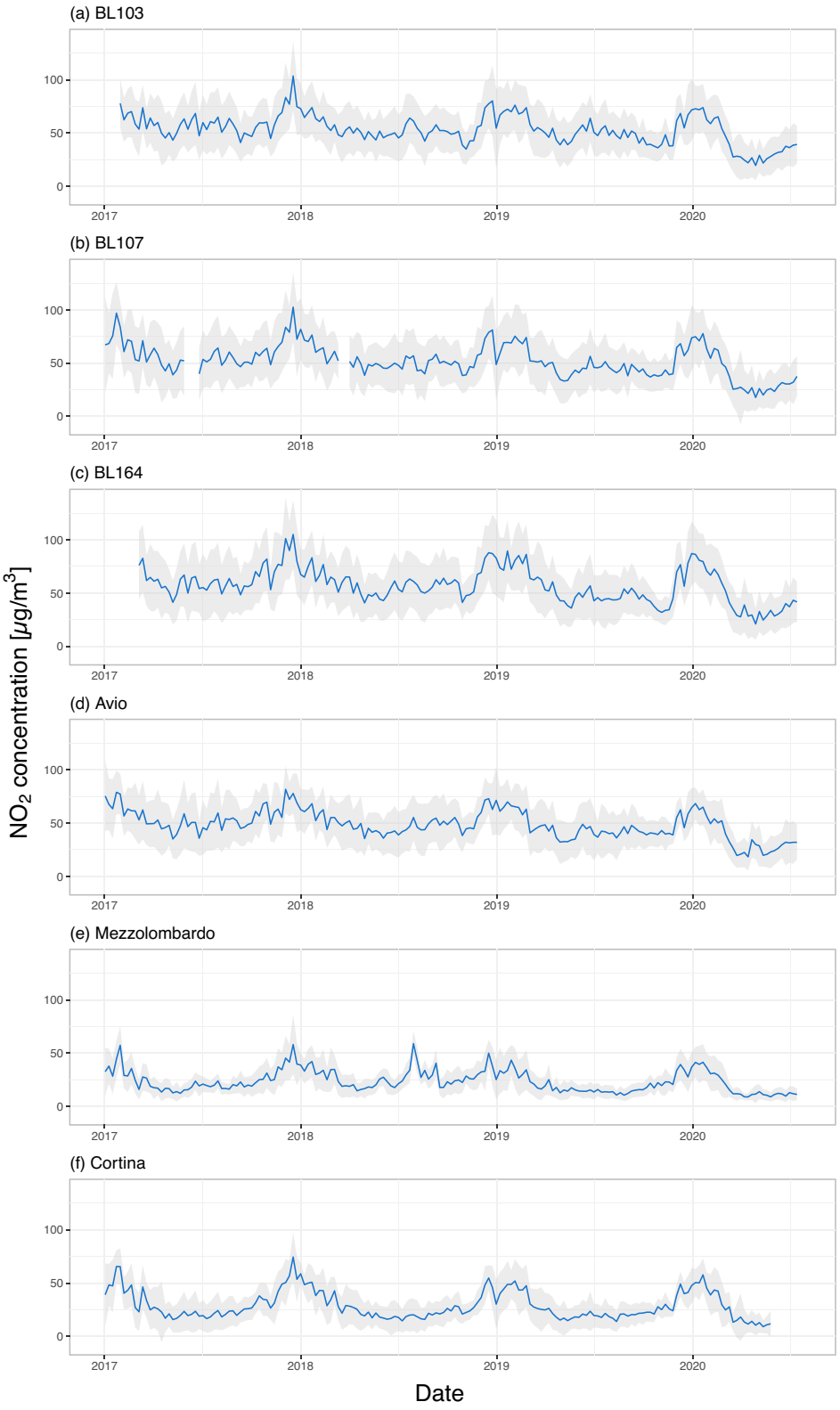

FIGURE 3 Measured NO_2 concentrations for all the stations. The blue line indicates the weekly mean and the grey shadow is the correspondent standard deviation. The time series start on 1st January 2017 and end on 20th July 2020, with the exception of Cortina, for which the available data extend only to the end of May 2020.

extremely close to the motorway, concentrations are generally higher at the traffic stations, with peaks of weekly average values exceeding 100 μg m^{-3}, while the maximum concentration measured by the rural stations, situated a few hundred metres away from the motorway, does not exceed 75 μg m^{-3}. In each plot an annual cycle is clearly visible: concentrations are higher in winter and lower in summer. As expected, the atmospheric stability characterizing wintertime hinders dispersion, which is, instead, promoted by the unstable atmospheric conditions typical of the summer period. The only exception to this cyclic behaviour is a summer peak measured at Mezzolombardo during 2018, whose cause is unknown. An important decrease in NO_2 concentrations during the first months of 2020 (the lockdown period) is visible in Figure 3, especially for the traffic stations. A decrease in the concentrations was expected due to the end of the winter period, but the comparison with the same months of the previous years reveals a more marked drop in 2020.

5.1.2 | Black carbon

Figure 4 shows the time series of the measured concentrations of the two BC components for BL103 and BL164. For both stations, BC_{ff} is significantly higher than BC_{bb}. This is an obvious consequence of their position: since they are both traffic stations, most of the BC is related to vehicular emissions. The BC_{bb} component, mainly related to domestic heating emissions, reaches significant values in winter (but still lower than BC_{ff}), while it is very low in the warm months. Similar to the NO_2 time series (Figure 3), also the measured concentrations of BC_{ff} exhibit a clear annual cycle, with higher values in winter and lower values in summer. The same analysis

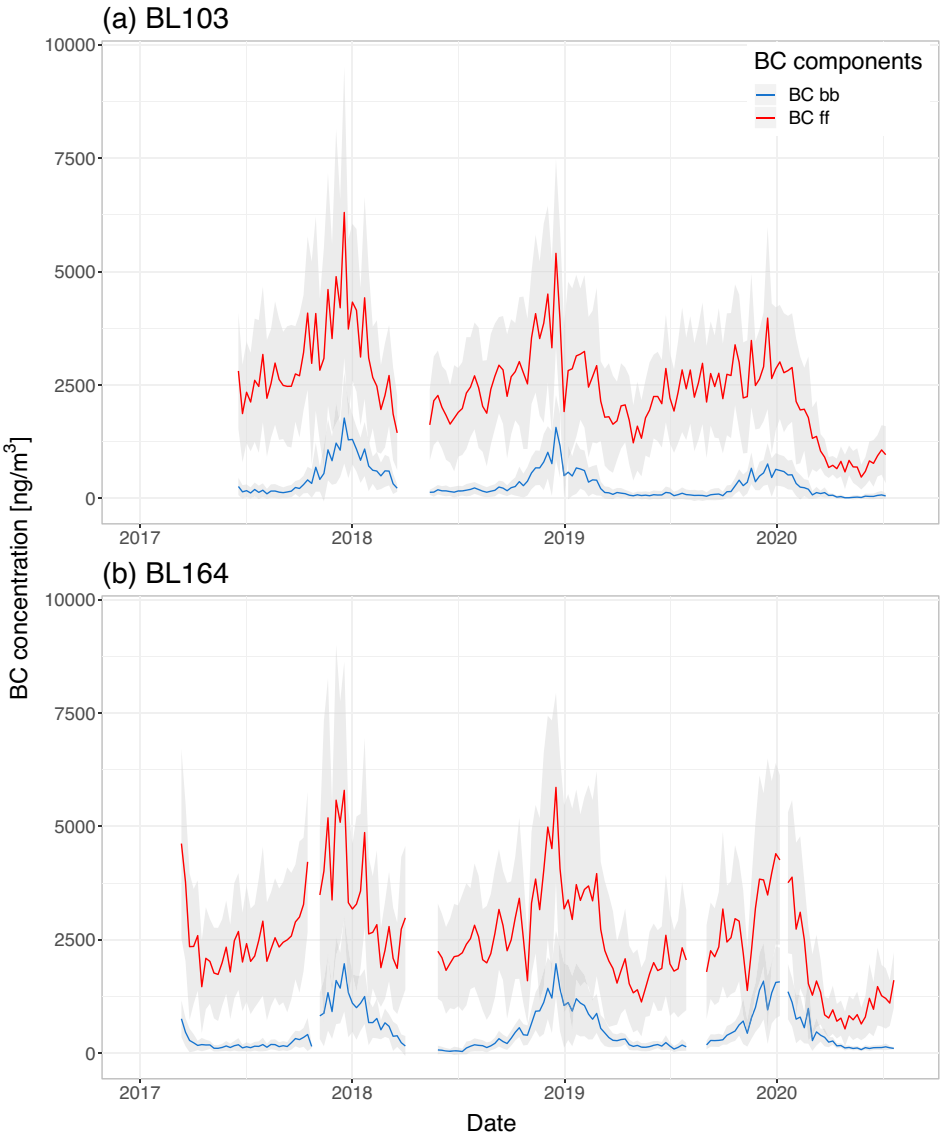

FIGURE 4 Measured BC concentrations at (a) BL103 and (b) BL164. The trends of biomass burning (bb) and fossil fuel (ff) components are shown in blue and red respectively. The time series start on March 2017 and end on 20th July 2020, the lines indicate weekly means and the shadowing the correspondent standard deviation.

performed for NO_2, comparing average observed concentrations in 2020 and in the three previous years in the periods from 1 January to 24 February (unaltered) and from 9 March to 2 June (lockdown), is repeated here for the two BC components, but only for BL164 (Table 4). BL103 is not considered due to the lack of data before mid-2017 and in spring 2018, which does not allow the calculation of robust statistics. During 2020 BC_{bb} concentrations increased in the unaltered period and decreased during the lockdown, with respect to the same periods of

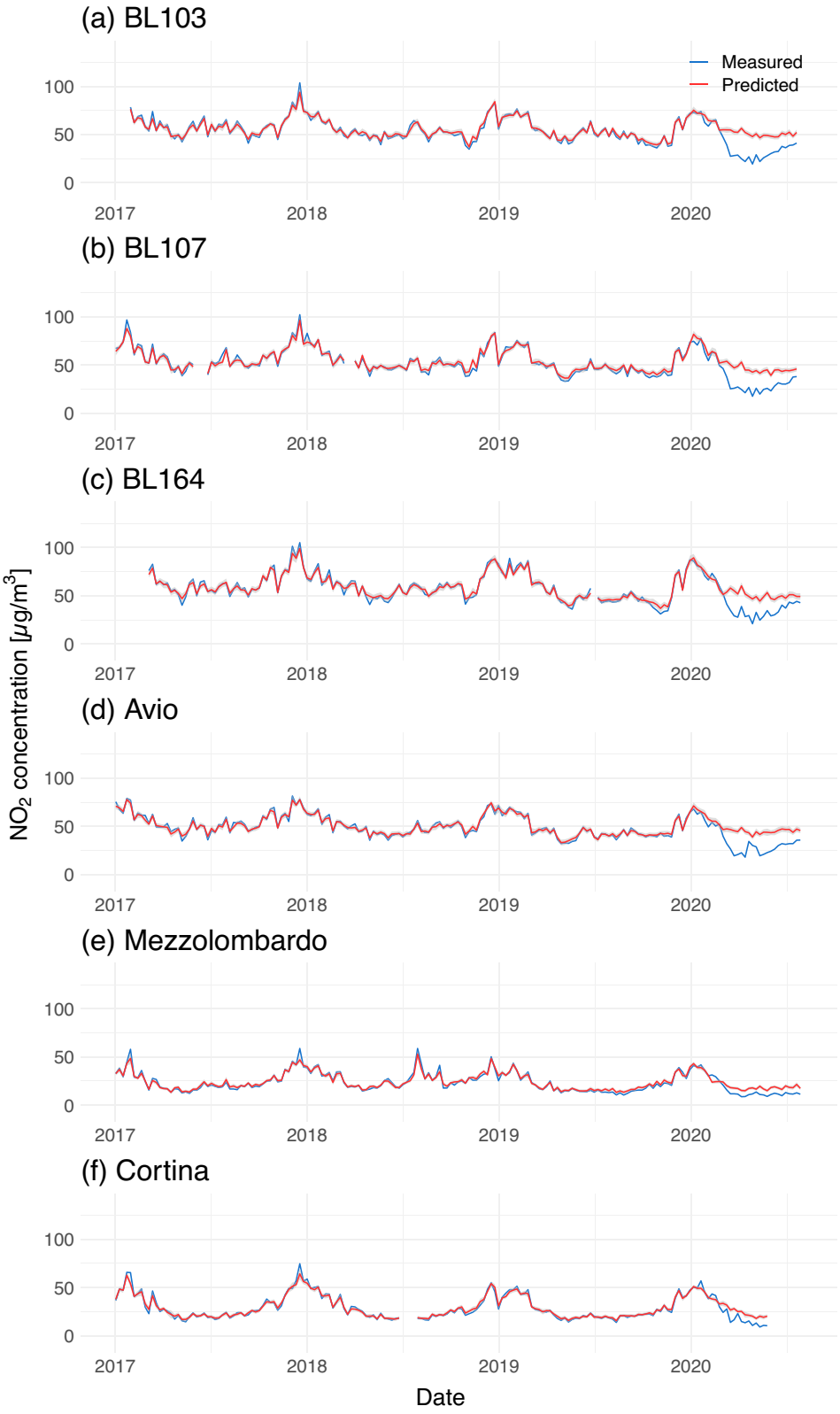

FIGURE 5 Predicted (red lines) and measured (blue lines) NO_2 concentrations for all the stations. Predictions were calculated for every day of the series but here, for graphical clarity, weekly means are shown. The predicted series are obtained by averaging the predictions of every tree and the grey shadow indicates the standard deviation.

the previous 3 years. However, the decrease during the lockdown is not particularly significant, given the low values of BC_{bb} concentrations during this period of the year. Moreover, the comparison with the BC_{ff} component reveals that, while BC_{ff} also slightly increased during the unaltered period, it experienced a much more significant drop (58%) in the lockdown period.

5.2 | Business-as-usual predicted concentrations

This section presents the results of the procedure described in Section 4 (steps 1–4), applied to the data introduced in Section 3, to obtain business-as-usual time series of NO_2 and BC concentrations. Moreover, in this section, also two significant outputs of the random forest algorithm, the partial dependence and the importance plots, are presented, along with the error estimators (R^2, RMSE). The partial dependence plots show the behaviour of the dependent variable (the concentration) as a function of each independent variable (meteorological and temporal ones). The importance plots show the ranking of the independent variables according to their importance, which is a measure of how much each of them affects the value of the dependent variable. The importance of a variable is calculated by considering each tree and the accuracy (RMSE) of its predictions on Out-of-Bag data, then randomly permuting the values of the variable in the Out-of-Bag data keeping all the other variables the same and finding the accuracy of the predictions using the permuted data (which is obviously lower than the one relative to the original Out-of-Bag data). The accuracy differences of all the trees are then averaged and normalized by the standard error, obtaining the importance. Hence, the variables having high importance are those that cause a high decrease in the accuracy of the predictions when their values are randomized and,

TABLE 5 R^2 and RMSE values evaluated for NO_2 and BC concentrations on the test set in the 2017–2019 period at all the stations.

NO_2		
Station	**R^2**	**RMSE [μg m^{-3}]**
BL103	0.85	6.99
BL107	0.89	8.26
BL164	0.89	7.99
Avio	0.86	7.32
Mezzolombardo	0.91	5.34
Cortina	0.92	6.46
BC		
Station	**R^2**	**RMSE [ng m^{-3}]**
BL164 BCff	0.89	527
BL164 BCbb	0.95	139

TABLE 6 Comparison between NO_2 and BC measured and predicted concentration values for all the stations in the unaltered and lockdown periods.

NO_2	**Unaltered (1 January–24 February)**	**Lockdown (9 March–2 June)**
BL103		
Predicted [μg m^{-3}]	68.9	51.23
Measured [μg m^{-3}]	67.6	26.7
Percentage change	−1.9%	−48.0%
BL107		
Predicted [μg m^{-3}]	70.5	46.7
Measured [μg m^{-3}]	67.5	25.3
Percentage change	−4.3%	−45.8%
BL164		
Predicted [μg m^{-3}]	77.3	51.8
Measured [μg m^{-3}]	76.5	30.6
Percentage change	−1.0%	−40.9%
Avio		
Predicted [μg m^{-3}]	62.6	44.4
Measured [μg m^{-3}]	58.8	24.6
Percentage change	−9.0%	−44.6%
Mezzolombardo		
Predicted [μg m^{-3}]	34.2	17.2
Measured [μg m^{-3}]	35.6	11.2
Percentage change	+4.1%	−34.9%
Cortina		
Predicted [μg m^{-3}]	44.6	22.3
Measured [μg m^{-3}]	47.0	13.6
Percentage change	+5.4%	−39.0%
BC	**Unaltered (1 January–24 February)**	**Lockdown (9 March–2 June)**
BL164 BC_{ff}		
Predicted [ng m^{-3}]	3815	2124
Measured [ng m^{-3}]	3469	883
Percentage change	−8.9%	−58.6%
BL164 BC_{bb}		
Predicted [ng m^{-3}]	1078	307
Measured [ng m^{-3}]	1061	218
Percentage change	−2.4%	−29.2%

conversely, they are the ones that cause a high increase in accuracy when they are correctly used for making predictions.

5.2.1 | NO_2

The time series of measured and predicted NO_2 concentrations are shown in Figure 5. In the time period from 2017 to 2019, the model is able to reproduce with good accuracy the measured concentrations; this is an obvious consequence of the training process: the model is built in such a way that it can reproduce the concentrations measured during these years. The accuracy of the model is quantitatively evaluated in Table 5, showing R^2 coefficients and RMSEs calculated using the test sets (i.e., the data not used for the training) in the time period from 2017 to 2019. All R^2 coefficients are around 0.9, indicating a good agreement between measurements and predictions, while RMSEs are, for NO_2, always less than 8.5 $\mu g\ m^{-3}$. The unaltered period in 2020 (as defined in Section 3.4), which is not included in the training dataset,

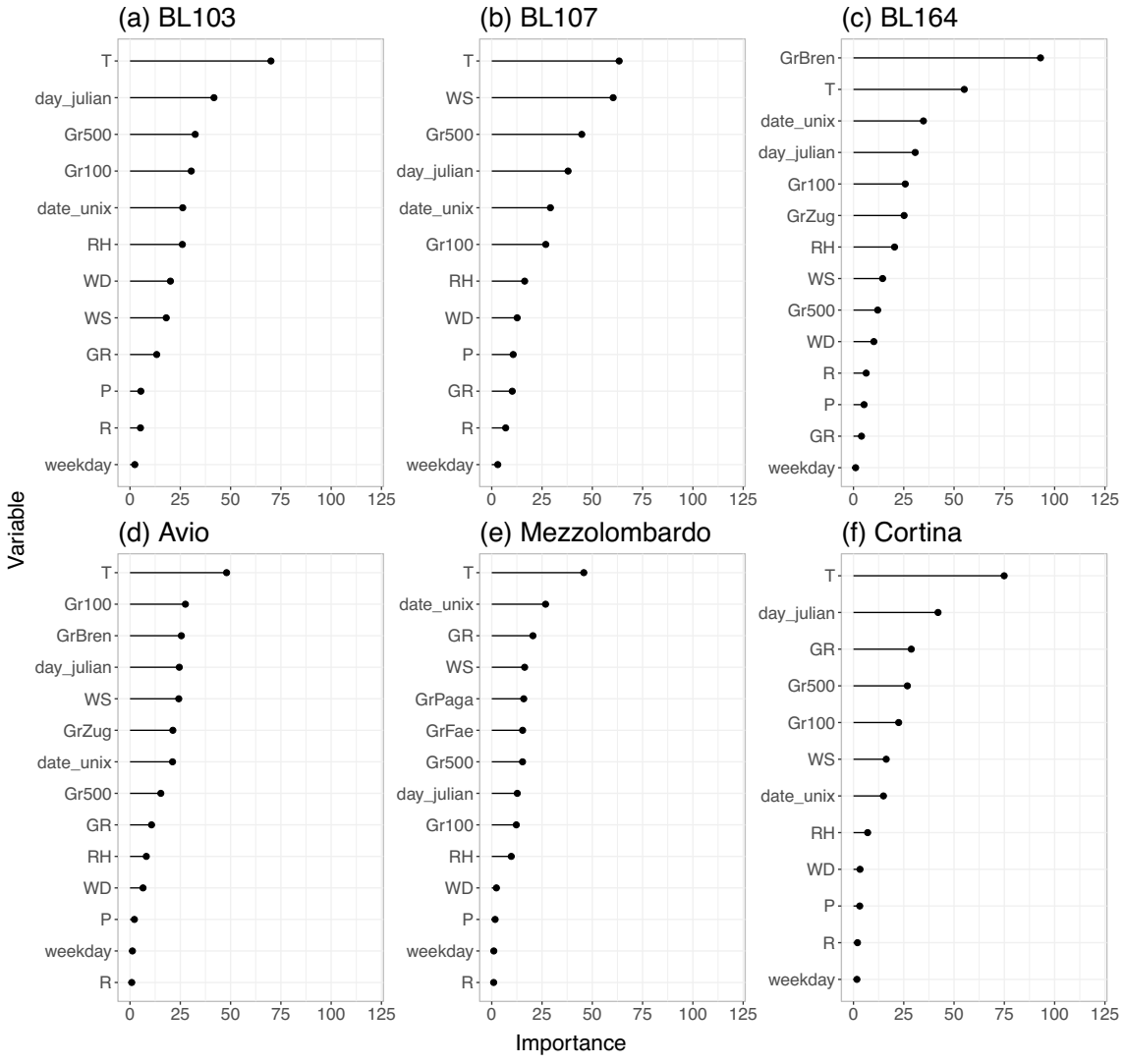

FIGURE 6 NO_2 importance plots for all the stations.

can also be considered as a validation period to evaluate the ability of the random forest model to correctly predict the observed concentrations. Figure 5 shows a good agreement between predictions and measurements during this period, highlighting that the model can be used to evaluate business-as-usual scenarios at all the stations analysed. This is confirmed by Table 6, which focuses on 2020 and presents the comparison between predicted and measured mean concentration values in the unaltered and lockdown periods. During the unaltered period, differences between observed and predicted concentrations are very small, generally between ±5%. On the other hand, both Figure 5 and Table 6 evidence that, during the lockdown period, the predicted concentrations are about 35%–45% higher than the measured ones. These predictions, neglecting the uncertainties connected to possible model errors, represent the concentrations that would have been measured, under the same meteorological conditions of 2020, if the emissions were identical to the previous years, that is, in a business-as-usual scenario. The differences between predicted and measured values are larger for the stations close to the motorway (BL103, BL107, BL164, Avio) than for the rural stations (Cortina, Mezzolombardo) and very similar to those presented in Table 4, referring to the comparison between the concentrations observed in 2020 and those measured in the previous 3 years. These results highlight that the observed decreases in the concentrations are not significantly affected by meteorological conditions, but can be mainly ascribed to the decrease in the emissions due to the restrictions introduced during the lockdown period. These results are comparable to what was found by Diémoz et al., 2021, who analysed the effects of lockdown measures on pollutant concentrations in the Aosta Valley, in the western Italian Alps, highlighting a concentration decrease of 40%–50%. Similarly, Putaud et al., 2021 found a decrease in NO_2 concentrations of 30% and 40% in rural and urban background stations in Lombardy (northern Italy), while Lonati & Riva, 2021 reported, in the Po Valley (northern Italy), a decrease in NO_2 concentrations of 35%–40%, with higher reductions, close to 50%, at high-volume-traffic sites in urban areas.

Finally, it can be observed that, especially at the traffic stations, the differences between observed and predicted concentrations tend to decrease at the end of the analysed period, due to the partial recovery of the traffic along the motorway (cf. Figure 2). Figure 6 shows the importance plots for the independent variables for all the stations. All the stations show a strong dependence on temperature and Julian day. The partial dependence plots for these two variables are shown in Figure 7: they both follow the annual cycle, with high concentrations on winter/cold days and low concentrations on summer/hot days. The partial dependence plot for temperature is similar to that found by Falocchi et al., 2021: roughly constant for temperatures lower than 2°C, then decreasing until 15°C and finally slightly increasing for higher temperatures. Figure 6 also indicates that the lapse rates have a major effect on the measured concentration values, especially for the traffic

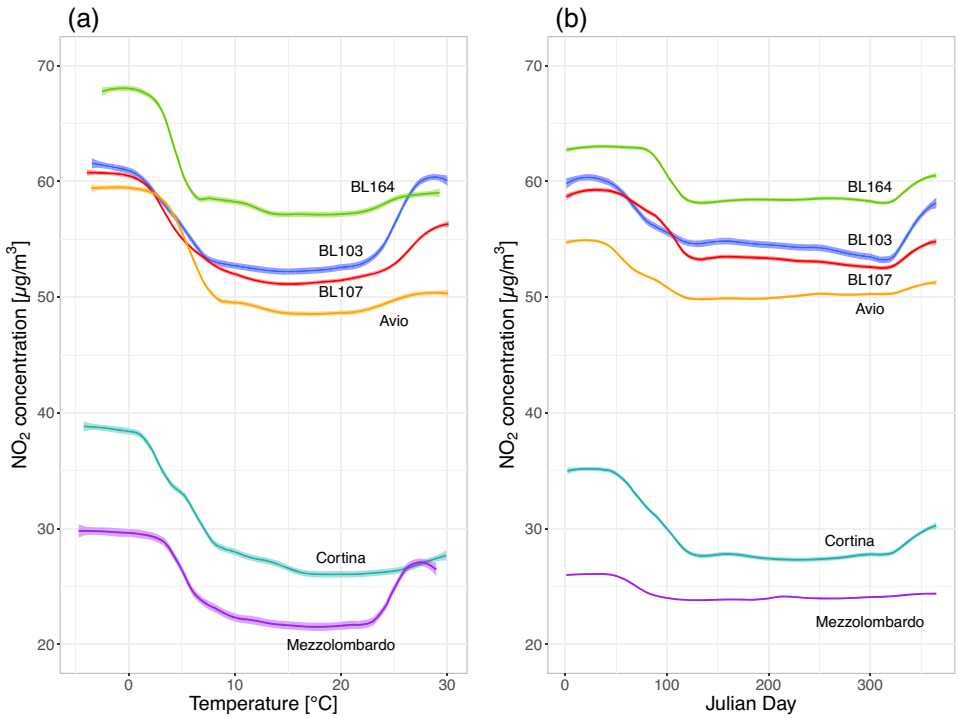

FIGURE 7 NO_2 partial dependence plots for (a) temperature and (b) Julian day for all the stations.

stations. In particular, the partial dependence plots for the lapse rates are shown in Figure 8: as expected, negative/low lapse rate values correspond to higher concentrations, on the contrary, when the lapse rate becomes more positive, concentrations decrease. Considering the southern stations, (Mezzolombardo, BL164 and Avio) the lapse rates calculated using data from surface weather stations at different heights present higher importance than the lapse rates calculated from the temperature profiler measurements, being the profiler representative of the meteorological conditions in another stretch of the valley. Wind speed turns out to be particularly important, especially at BL107 and Mezzolombardo. The partial dependence plot for this variable is shown in Figure 9a: with strong wind speed, concentration values decrease because of shear mixing effects. Finally, Figure 9b shows the partial dependence plot for global solar radiation, which is important for Cortina and Mezzolombardo. In this case, concentrations decrease with increasing radiation, as high radiation values occur during summer when dispersion is more efficient.

5.2.2 | Black carbon

The random forest algorithm was applied to both BC_{bb} and BC_{ff} components. Only results for BL164 are

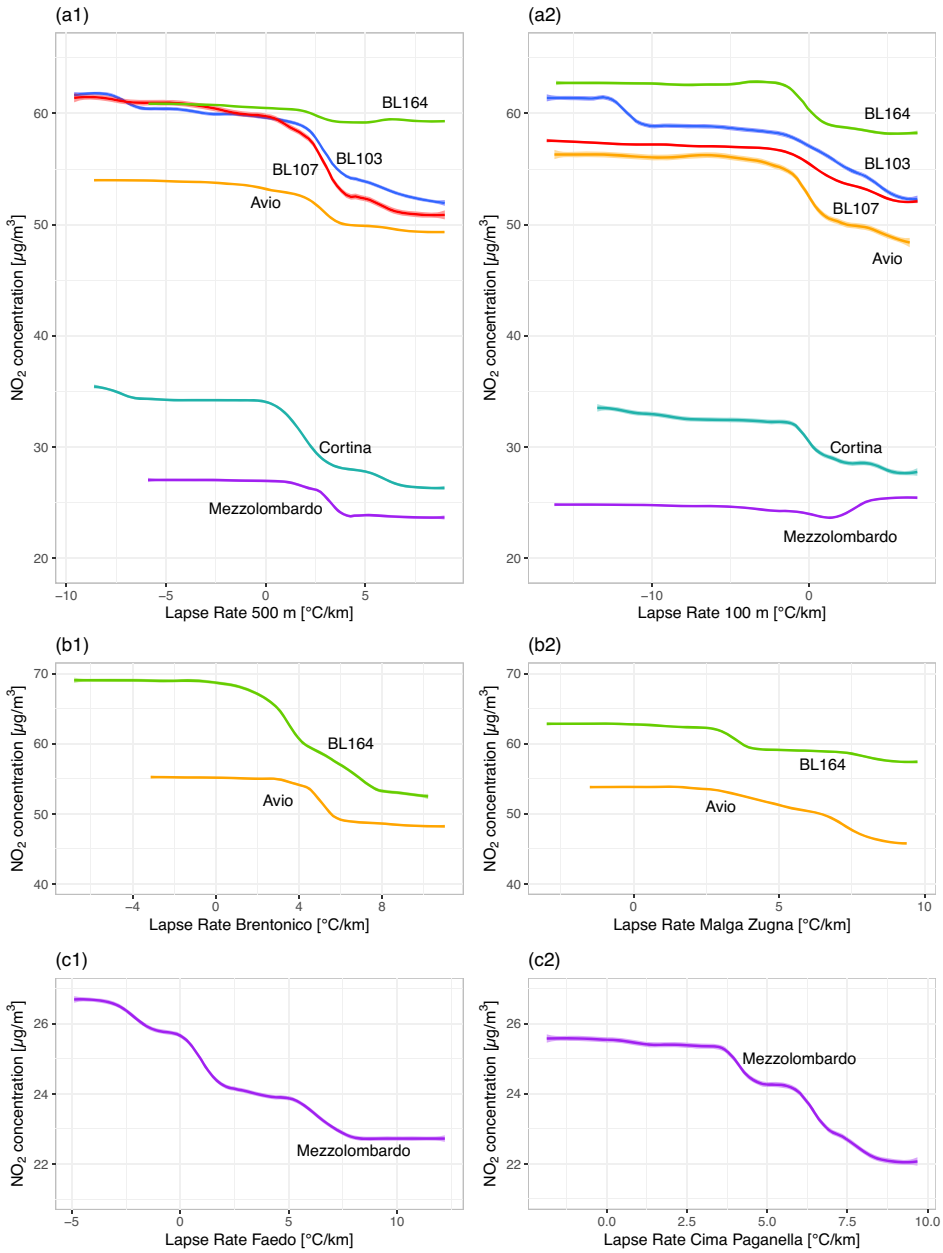

FIGURE 8 NO_2 partial dependence plots for the lapse rates for all the stations: (a1) lapse rate calculated from the temperature profiler for the lowest 500 m AGL, (a2) lapse rate calculated from the temperature profiler for the lowest 100 m AGL, (b1) lapse rate calculated using measurements at Brentonico, (b2) lapse rate calculated using measurements at Malga Zugna, (c1) lapse rate calculated using measurements at Faedo, (c2) lapse rate calculated using measurements at Cima Paganella.

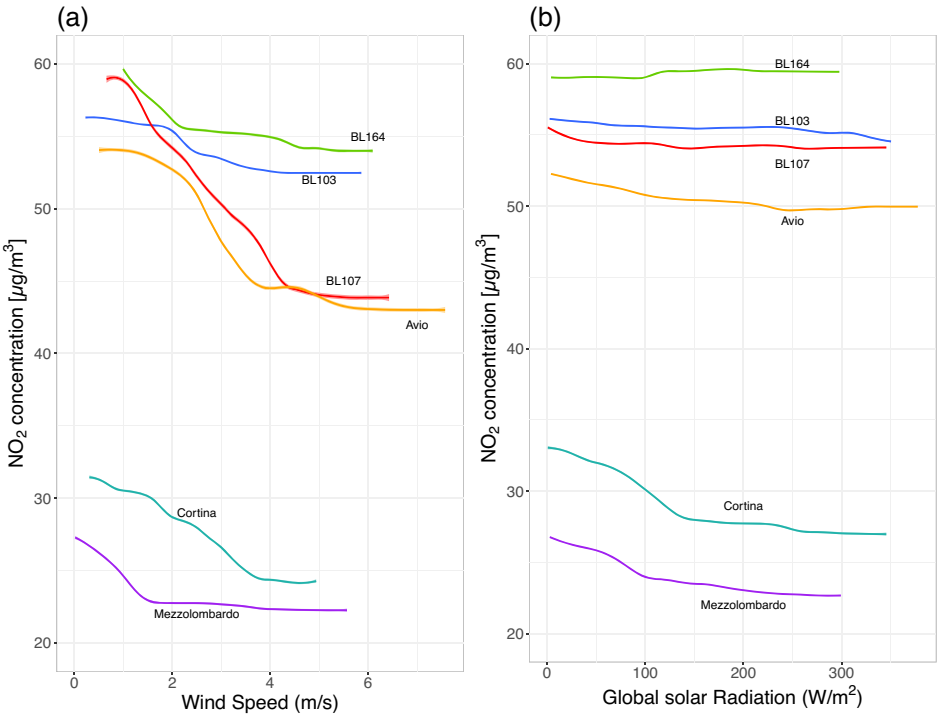

FIGURE 9 NO_2 partial dependence plots for (a) wind speed and (b) global solar radiation for all the stations.

presented here, since the lack of data before mid-2017 and in spring 2018 at BL103 did not allow for satisfactory training of the random forest algorithm at this air quality station. The time series of measured and predicted concentrations of the two BC components at this station are shown in Figure 10. As for NO_2, the machine learning algorithm is able to reasonably reproduce the observed concentrations of both BC components both in the training period from 2017 to 2019 and during the unaltered period in 2020, highlighting that this methodology can be safely adopted to evaluate the effects of the lockdown restrictions on BC concentrations. The RMSE and R^2 values evaluated on the test set in the 2017–2019 period are shown in Table 5, highlighting, also in this case, a satisfactory agreement between measurements and predictions. During the lockdown period, the predicted concentrations are always higher than the observations for both components (Table 6). This behaviour is particularly evident for BC_{ff}, which, as expected, behaves similarly to NO_2, since both these pollutants mainly originate from traffic. The BC_{bb} component shows a smaller but significant difference between predictions and measurements. The decrease in concentrations observed during the lockdown period is also in this case comparable to that evaluated from observations (Table 4) for BC_{ff}, while slightly higher for BC_{bb}. However, accurate evaluations of the trend of the BC_{bb} component can be problematic along a busy road, since in this context it represents a small fraction of the total BC and, as a consequence, the uncertainties connected to the application of the random

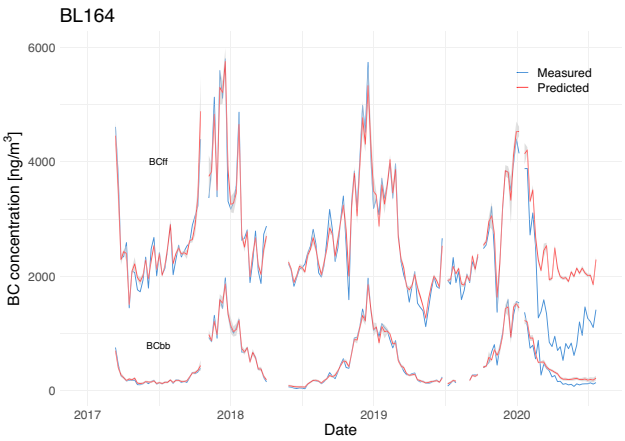

FIGURE 10 Predicted (red lines) and measured (blue lines) BC concentrations for BL164. Predictions were calculated for every day of the series but here, for graphical clarity, weekly means are shown. The predicted series are obtained by averaging the predictions of every tree and the grey shadow indicates the standard deviation.

forest algorithm may be proportionally more significant. Moreover, the measurements of the two main BC components can be compromised by the presence of brown carbon, which is another type of light-absorbing carbonaceous aerosol (Andreae & Gelencsér, 2006). Similarly to BC, brown carbon can be produced by the combustion of biomass and fossil fuels, but can also be originated from soils and bioaerosols or formed through

secondary processes and photo-activated chemical reactions (Wong et al., 2017). Brown carbon particles have a brown-yellow colour and their absorption efficiency, with respect to BC, is negligible at visible wavelengths but becomes significant towards UV wavelengths (Yan et al., 2018). It is then possible that the presence of this brown carbon component affected the measurements, especially the ones made at 470 nm (the shortest wavelength), and this affected in turn the calculated fractions of BC_{bb} and BC_{ff}.

The results obtained in the present study confirm, as expected, that lockdown measures had a stronger impact on BC_{ff}, as shown for example by Goel et al., 2021 in Dehli, even if our findings cannot be generalized, as only BC data from a traffic site were analysed. However, results highlight that, close to the motorway, also BC_{bb} experienced a slight decrease, differently from what was suggested by Gualtieri et al., 2020, who analysed PM data in six Italian cities.

The importance plots for the two BC components are shown in Figure 11: temperature, Julian day and lapse rates are among the variables that have the greatest impact on BC concentrations, for both components, similar to NO_2. For these variables, the partial dependence trends (Figures 12 and S2) are overall similar to those obtained for NO_2 (Figures 7 and 8). Considering the partial dependence plots for the temperature and the Julian day (Figure 12), it is interesting to notice that BC_{bb} displays a completely flat behaviour at high temperatures, in contrast with the increase occurring at about 25°C for both NO_2 and BC_{ff}. This is caused by the fact that, with high temperatures, domestic heating is basically absent, and, consequently, concentrations of BC_{bb} remain low and constant. On the other hand, the similar behaviour of NO_2 and BC_{ff} partial dependence plots confirms that these two pollutants present the same main emission source, that is, vehicular traffic. Figure 11 highlights that wind speed has significant importance as well, especially for BC_{ff}.

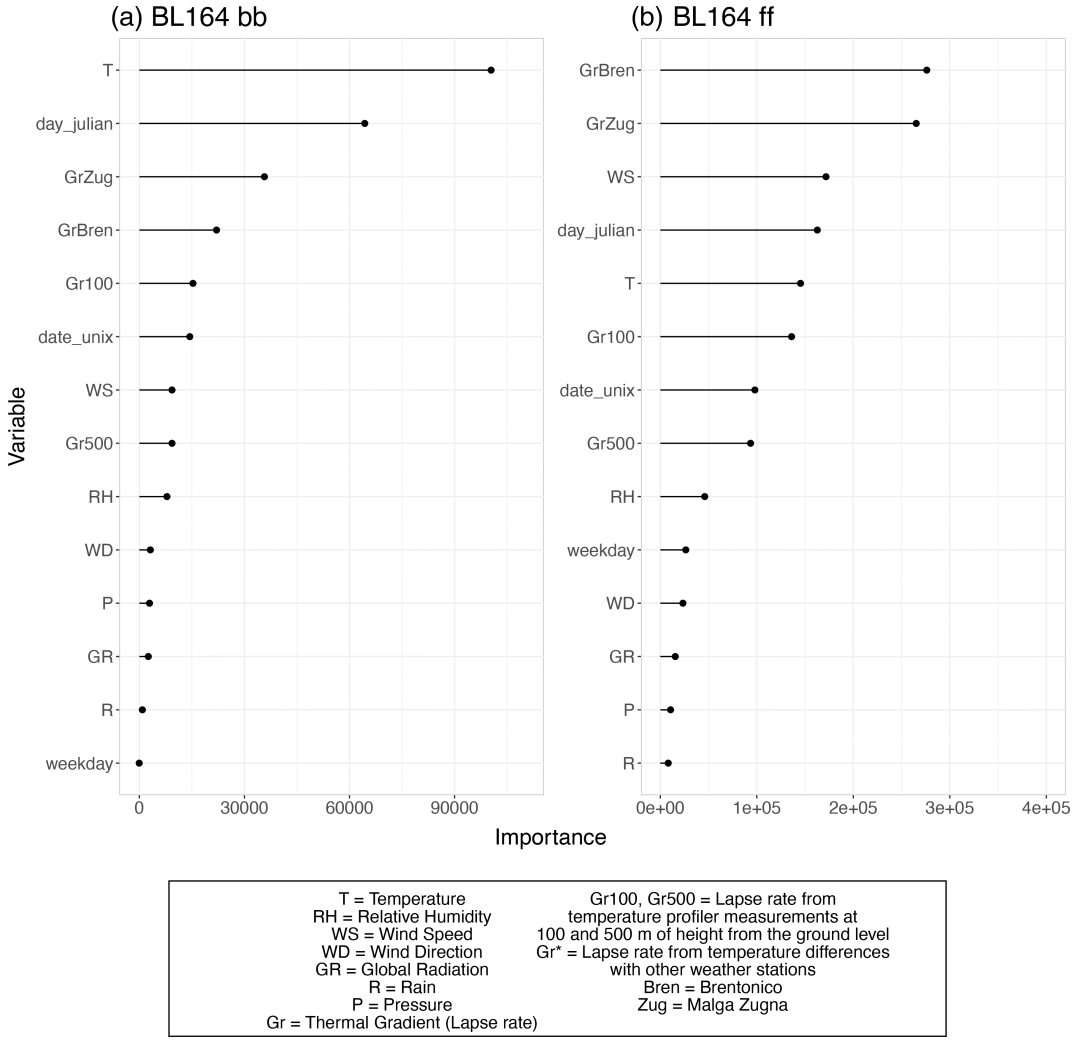

FIGURE 11 BC importance plots for BL164.

The partial dependence plots for this variable and for global solar radiation (Figure S3) once again resemble those found for NO_2 (Figure 9), with concentrations decreasing when wind speed and global solar radiation values increase.

5.3 | Normalized concentrations

The machine learning algorithm was also applied to produce meteorologically normalized time series (Section 4, steps 1–3, 5) of both NO_2 and BC concentrations. In this section, one normalized time series for each pollutant (BL103 for NO_2 and BL164 for BC) is presented and commented on.

5.3.1 | NO_2

The NO_2 normalized time series for BL103 is shown in Figure 13a. Being the effects of the meteorological variability on observed concentrations removed, the normalized time series is much smoother than the original one, and in particular, the annual cycle, which was clearly evident in Figure 3, is no longer appreciable. For the year 2020, the normalized series reflects the progressive introduction of restrictions to circulation. In fact, the concentration is roughly constant until the end of February, and then it starts to decrease when the first restriction measures were introduced. On the other hand, on 9th March, in connection with the beginning of the lockdown period, an abrupt drop in the normalized concentrations can be clearly seen. During this phase, the normalized concentrations remain constant at low levels, increasing only after 3rd June, that is, the beginning of the upturn period. The drop in the normalized concentrations on 9th March is around 12 μg m^{-3}. On the other hand, in the time span of 2017–2019, the normalized concentrations experience a progressive decrease of about 7 μg m^{-3}, probably due to the renewal of the car fleet observed along this motorway (De Biasi, 2021). In fact, newer vehicles, especially heavy-duty vehicles, produce lower emissions. It can be then stated that the results obtained with the abrupt emission diminution caused by the lockdown will be achieved in around 5 years with the current rate of reduction of the emissions due to the car fleet renewal. Grange et al., 2021 presented the results of a similar estimate for different European cities, concluding that the effects of the lockdown will be achieved on average in 7.6 years considering the current rate of NO_2 reduction. The shorter time period estimated here may be due to the fact that the long-term decrease in NO_2 concentrations is more significant in the present case study, as NO_2 concentrations close to the motorway are strongly influenced by the emissions of heavy vehicles, which experienced a strong reduction in the last few years after the introduction of the Euro VI technology (Grigoratos et al., 2019).

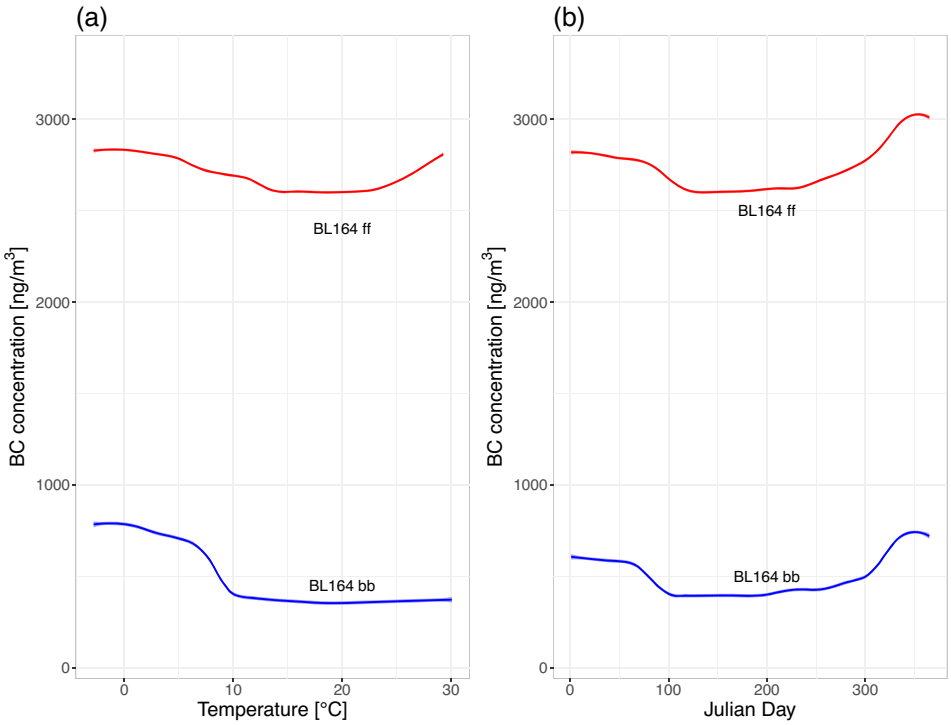

FIGURE 12 BC partial dependence plots for (a) temperature and (b) Julian day for BL164.

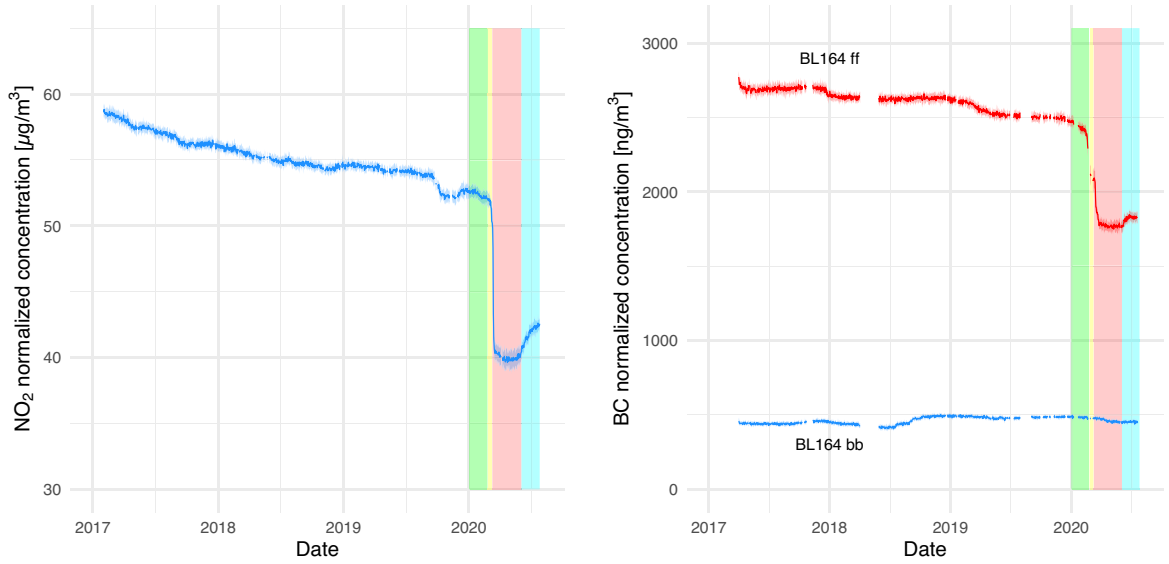

FIGURE 13 Normalized series for (a) NO_2 at BL103 and (b) the two BC components at BL164. Background colours indicate the periods individuated in Section 3.4: unaltered (green), transition (yellow), lockdown (red) and upturn (cyan). The solid lines represent the mean of the 20 iterations of the random forest model and the shadowing shows the standard deviation.

5.3.2 | Black carbon

Figure 13b shows the normalized time series of the two BC components for BL164. In the first months of 2020, BC_{ff} shows a behaviour quite similar to the NO_2 normalized series. In particular, after an initial phase in which normalized concentrations are almost constant, they slightly decrease during the transition period, until the abrupt drop on 9th March. Normalized concentrations then remain almost constant at low values during the lockdown period, and slightly increase at the very end of the series. The normalized concentrations of BC_{bb}, instead, show negligible variations throughout the same time period. This confirms the considerations reported in the previous sections: BC_{ff}, strongly depending on traffic, is heavily influenced by the lockdown restrictions, whereas the effects on BC_{bb}, depending mainly on space heating, are less significant. Similar to NO_2, in the time span of 2017–2019 the normalized concentrations of BC_{ff} progressively decrease by about 200 ng m^{-3}, thanks to the renewal of the car fleet. On the other hand, the drop due to the lockdown is around 700 ng m^{-3}, so proportionally more significant than for NO_2. Finally, no significant trends for BC_{bb} are appreciable in the time span of 2017–2019, highlighting that the emissions of this pollutant have been almost constant during this period and that no long-term trend is present for this variable.

6 | CONCLUSIONS

Data from six air quality stations located in the Alpine Adige valley were analysed in order to evaluate the effects of the restrictions introduced to prevent the spread of the COVID-19 pandemic on NO_2 and black carbon concentrations at different distances from the A22 Italian motorway. Two different black carbon components were considered: the one related to fossil fuel combustion (BC_{ff}) and the one related to biomass burning (BC_{bb}). The analysis was performed considering different time periods, defined on the basis of the changes in the restrictions imposed by the government and the consequent variations in the traffic load along the motorway. In order to take into account the effects of the variability of meteorological conditions on the measured concentrations, a random forest algorithm was applied, to obtain business-as-usual and meteorologically normalized time series of both NO_2 and BC concentrations.

The analysis of observed concentrations highlighted that, during the period without restrictions, both NO_2 and BC concentrations in 2020 presented similar values to those relative to the same period of the previous 3 years. On the other hand, during the period with the heaviest restrictions, NO_2 concentrations dropped by 38–48% with respect to the previous 3 years, BC_{ff} (mainly related to traffic) exhibited similar behaviour, plummeting by 58%, whereas BC_{bb} (mainly produced by domestic heating) experienced only a slight decrease, highlighting that the emission sources of this pollutant were not significantly affected by the restrictions. Considering NO_2, the highest reductions were observed at the stations located close to the motorway, which were most affected by the huge traffic drop. However, the concentration decrease was significant also considering rural background stations, highlighting a general reduction of

concentration levels on the floor of the Adige valley. These results were confirmed by the predictive business-as-usual time series, which allowed for obtaining an estimate of the daily concentration values that would have been measured in 2020 if the emissions were comparable to those of the previous 3 years. It was found that, for both NO_2 and BC, observed and predicted concentrations presented similar values in the first period of 2020 when the restrictions had not yet been introduced and the traffic load along the motorway was similar to the previous 3 years. The good agreement between observed and predicted values during this testing period assured that this methodology can be safely adopted to evaluate the effects of the restrictions on pollutant concentrations. On the other hand, the predicted values were higher than the measured ones during the period with the restrictions for all the pollutants considered here. For NO_2 and BC_{ff} the differences between measurements and predictions were huge, as expected, since both these pollutants are mainly produced by vehicular traffic. Moreover, these values were very similar to those obtained from the first analysis of observed concentrations. For BC_{bb}, the difference found was smaller, especially considering absolute values, due to the low concentrations of this BC component in spring. Considering normalized time series, the analysis for NO_2 showed an abrupt drop in correspondence of the day on which the heavy restrictions were introduced. This drop was found to be equivalent to the diminution that would be obtained in 5 years following the current rate of concentration decrease induced by the vehicle fleet renewal. The BC_{ff} normalized time series was very similar, with an important drop in connection with the beginning of the lockdown period, confirming that these two pollutants share the same main emission source: the traffic. The BC_{bb} normalized trend, instead, showed no significant variations during the lockdown period, indicating the different origins of this pollutant.

The results found in the present work confirm that the COVID-19 lockdown measures had a strong impact on the emissions of traffic-related pollutants, with a significant decrease in concentrations also at rural background stations, located at a considerable distance from the main sources. This highlights that the reduction of traffic-related emissions has a positive impact not only in the near-road environment but also on a wider spatial scale, including the whole floor of a main Alpine valley. However, it is also clear that policies aiming at improving air quality conditions should take into account also other factors, including biomass burning, which still remains one of the most important pollutant sources in Alpine valleys (Urgnani et al., 2022).

AUTHOR CONTRIBUTIONS

Elena Bertazza: Data curation (lead); formal analysis (lead); investigation (equal); software (equal); visualization (lead); writing – original draft (lead). **Andrea Bisignano:** Conceptualization (equal); investigation (equal); methodology (equal); supervision (equal); writing – review and editing (equal). **Marco Falocchi:** Methodology (equal); software (lead). **Lorenzo Giovannini:** Conceptualization (lead); investigation (equal); methodology (equal); project administration (lead); supervision (lead); writing – review and editing (lead).

ACKNOWLEDGEMENTS

The authors would like to thank all the partners of the BrennerLEC project for their technical support and useful suggestions. In particular, special thanks go to Roberto Cavaliere (NOI Techpark), Ilaria De Biasi (Autostrada del Brennero S.p.A.), Valentina Miotto (APPATN), Gianluca Antonacci and Ilaria Todeschini (CISMA Srl), Massimo Guariento and Patrick Dalpiaz (APPABZ). The authors would like to acknowledge The Environmental Protection Agency of the Autonomous Province of Trento (APPATN), the Environment and Climate Protection Agency of the Autonomous Province of Bolzano (APPABZ), the Edmund Mach Foundation and Meteotrentino for providing air quality and meteorological data from their stations.

FUNDING INFORMATION

This research was funded by the European Commission through the LIFE program, grant number LIFE15 ENV/IT/000281 ("BrennerLEC" project).

ORCID

Elena Bertazza https://orcid.org/0000-0003-0653-2131
Lorenzo Giovannini https://orcid.org/0000-0003-1650-0344

REFERENCES

Andreae, M.O. & Gelencsér, A. (2006) Black carbon or brown carbon? The nature of light-absorbing carbonaceous aerosols. *Atmospheric Chemistry and Physics*, 6, 3131–3148. Available from: https://doi.org/10.5194/acp-6-3131-2006

Anh, V., Duc, H. & Azzi, M. (1997) Modeling anthropogenic trends in air quality data. *Journal of the Air & Waste Management Association*, 47, 66–71. Available from: https://doi.org/10.1080/10473289.1997.10464406

Bisignano, A., Carotenuto, F., Zaldei, A. & Giovannini, L. (2022) Field calibration of a low-cost sensors network to assess traffic-related air pollution along the Brenner highway. *Atmospheric Environment*, 275, 119008. Available from: https://www.sciencedirect.com/science/article/pii/S1352231022000735

Breiman, L. (1996) Bagging predictors. *Machine Learning*, 24, 123–140. Available from: https://doi.org/10.1007/bf00058655

Clements, C.B., Whiteman, C.D. & Horel, J.D. (2003) Cold-air-pool structure and evolution in a mountain basin: Peter sinks, Utah. *Journal of Applied Meteorology*, 42, 752–768. Available from: https://doi.org/10.1175/1520-0450(2003)042%3C0752:CSAEIA%3E2.0.CO;2

De Biasi, I. (2021) The lower emissions Brenner corridor. *The Project Repository Journal*, 10, 86–89. Available from: https://doi.org/10.54050/prj10086089

de Franceschi, M. & Zardi, D. (2009) Study of wintertime high pollution episodes during the Brenner-south ALPNAP measurement campaign. *Meteorology and Atmospheric Physics*, 103, 237–250. Available from: https://doi.org/10.1007/s00703-008-0327-2

Deolal, S.P., Brunner, D., Steinbacher, M., Weers, U. & Staehelin, J. (2012) Long-term in situ measurements of NO_x and NO_y at Jungfraujoch 1998–2009: time series analysis and evaluation. *Atmospheric Chemistry and Physics*, 12, 2551–2566. Available from: https://doi.org/10.5194/acp-12-2551-2012

Diémoz, H., Magri, T., Pession, G., Tarricone, C., Tombolato, I.K.F., Fasano, G. et al. (2021) Air quality in the Italian northwestern Alps during year 2020: assessment of the COVID-19 «lockdown effect» from multi-technique observations and models. *Atmosphere*, 12, 1006. Available from: https://www.mdpi.com/2073-4433/12/8/1006

Falocchi, M., Zardi, D. & Giovannini, L. (2021) Meteorological normalization of NO2 concentrations in the province of Bolzano (Italian Alps). *Atmospheric Environment*, 246, 118048. Available from: https://doi.org/10.1016/j.atmosenv.2020.118048

Felzer, B.S., Cronin, T., Reilly, J.M., Melillo, J.M. & Wang, X. (2007) Impacts of ozone on trees and crops. *Comptes Rendus Geoscience*, 339, 784–798. Available from: https://doi.org/10.1016/j.crte.2007.08.008

Fenech, S., Aquilina, N.J. & Vella, R. (2021) COVID-19-related changes in NO2 and O3 concentrations and associated health effects in Malta. *Frontiers in Sustainable Cities*, 3, 631280. Available from: https://doi.org/10.3389/frsc.2021.631280

Frampton, M.W., Boscia, J., Roberts, N.J., Azadniv, M., Torres, A., Cox, C. et al. (2002) Nitrogen dioxide exposure: effects on airway and blood cells. *American Journal of Physiology. Lung Cellular and Molecular Physiology*, 282, L155–L165. Available from: https://doi.org/10.1152/ajplung.2002.282.1.l155

Giovannini, L., Ferrero, E., Karl, T., Rotach, M.W., Staquet, C., Castelli, S.T. et al. (2020) Atmospheric pollutant dispersion over complex terrain: challenges and needs for improving air quality measurements and modeling. *Atmosphere*, 11, 646. Available from: https://doi.org/10.3390/atmos11060646

Goel, V., Hazarika, N., Kumar, M., Singh, V., Thamban, N.M. & Tripathi, S.N. (2021) Variations in black carbon concentration and sources during COVID-19 lockdown in Delhi. *Chemosphere*, 270, 129435. Available from: https://www.sciencedirect.com/science/article/pii/S004565352033633X

Grange, S.K. & Carslaw, D.C. (2019) Using meteorological normalisation to detect interventions in air quality time series. *Science of the Total Environment*, 653, 578–588. Available from: https://doi.org/10.1016/j.scitotenv.2018.10.344

Grange, S.K., Carslaw, D.C., Lewis, A.C., Boleti, E. & Hueglin, C. (2018) Random forest meteorological normalisation models for swiss PM10 trend analysis. *Atmospheric Chemistry and Physics*, 18, 6223–6239. Available from: https://doi.org/10.5194/acp-18-6223-2018

Grange, S.K., Lee, J.D., Drysdale, W.S., Lewis, A.C., Hueglin, C., Emmenegger, L. et al. (2021) COVID-19 lockdowns highlight a risk of increasing ozone pollution in European urban areas. *Atmospheric Chemistry and Physics*, 21, 4169–4185. Available from: https://doi.org/10.5194/acp-21-4169-2021

Grigoratos, T., Fontaras, G., Giechaskiel, B. & Zacharof, N. (2019) Real world emissions performance of heavy-duty euro VI diesel vehicles. *Atmospheric Environment*, 201, 348–359. Available from: https://doi.org/10.1016/j.atmosenv.2018.12.042

Gualtieri, G., Brilli, L., Carotenuto, F., Vagnoli, C., Zaldei, A. & Gioli, B. (2020) Quantifying road traffic impact on air quality in urban areas: a Covid19-induced lockdown analysis in Italy. *Environmental Pollution*, 267, 115682. Available from: https://www.sciencedirect.com/science/article/pii/S0269749120363715

Guevara, M., Jorba, O., Soret, A., Petetin, H., Bowdalo, D., Serradell, K. et al. (2021) Time-resolved emission reductions for atmospheric chemistry modelling in Europe during the COVID-19 lockdowns. *Atmospheric Chemistry and Physics*, 21, 773–797. Available from: https://doi.org/10.5194/acp-21-773-2021

Henneman, L.R., Holmes, H.A., Mulholland, J.A. & Russell, A.G. (2015) Meteorological detrending of primary and secondary pollutant concentrations: method application and evaluation using long-term (2000–2012) data in Atlanta. *Atmospheric Environment*, 119, 201–210. Available from: https://doi.org/10.1016/j.atmosenv.2015.08.007

Ho, T.K. (1995) Random decision forests. In: *Proceedings of 3rd international conference on document analysis and recognition*, 14-16 August 1995. Montreal: IEEE Computer Society Press. Available from: https://doi.org/10.1109/icdar.1995.598994

Hudda, N., Simon, M.C., Patton, A.P. & Durant, J.L. (2020) Reductions in traffic-related black carbon and ultrafine particle number concentrations in an urban neighborhood during the COVID-19 pandemic. *Science of the Total Environment*, 742, 140931. Available from: https://www.sciencedirect.com/science/article/pii/S0048969720344600

Kotsiantis, S.B. (2013) Decision trees: a recent overview. *Artificial Intelligence Review*, 39, 261–283. Available from: https://doi.org/10.1007/s10462-011-9272-4

Laeremans, M., Dons, E., Avila-Palencia, I., Carrasco-Turigas, G., Orjuela-Mendoza, J., Anaya-Boig, E. et al. (2018) Black carbon reduces the beneficial effect of physical activity on lung function. *Medicine and Science in Sports and Exercise*, 50, 1875–1881. Available from: https://doi.org/10.1249/mss.0000000000001632

Liu, Y., Wang, Y., Cao, Y., Yang, X., Zhang, T., Luan, M. et al. (2021) Impacts of COVID-19 on black carbon in two representative regions in China: insights based on online measurement in Beijing and Tibet. *Geophysical Research Letters*, 48, e2021GL092770. Available from: https://doi.org/10.1029/2021GL092770

Lonati, G. & Riva, F. (2021) Regional scale impact of the COVID-19 lockdown on air quality: gaseous pollutants in the Po Valley, northern Italy. In: *Atmosphere*, 12, 264. Available from: https://www.mdpi.com/2073-4433/12/2/264

Lu, H.-C. & Chang, T.-S. (2005) Meteorologically adjusted trends of daily maximum ozone concentrations in Taipei Taiwan.

Atmospheric Environment, 39, 6491–6501. Available from: https://doi.org/10.1016/j.atmosenv.2005.06.007

Magalhaes, S., Baumgartner, J. & Weichenthal, S. (2018) Impacts of exposure to black carbon, elemental carbon, and ultrafine particles from indoor and outdoor sources on blood pressure in adults: a review of epidemiological evidence. *Environmental Research*, 161, 345–353. Available from: https://doi.org/10.1016/j.envres.2017.11.030

Mallet, M.D. (2020) Meteorological normalisation of PM10 using machine learning reveals distinct increases of nearby source emissions in the Australian mining town of Moranbah. *Atmospheric Pollution Research*, 12, 23–35. Available from: https://doi.org/10.1016/j.apr.2020.08.001

Mayr, G.J. & Armi, L. (2010) The influence of downstream diurnal heating on the descent of flow across the sierras. *Journal of Applied Meteorology and Climatology*, 49, 1906–1912. Available from: https://doi.org/10.1175/2010jamc2516.1

Neff, W.D. & King, C.W. (1989) The accumulation and pooling of drainage flows in a large basin. *Journal of Applied Meteorology*, 28, 518–529. Available from: https://doi.org/10.1175/1520-0450(1989)028%3C0518:TAAPOD%3E2.0.CO;2

Putaud, J.-P., Pozzoli, L., Pisoni, E., Martins Dos Santos, S., Lagler, F., Lanzani, G. et al. (2021) Impacts of the COVID-19 lockdown on air pollution at regional and urban background sites in northern Italy. *Atmospheric Chemistry and Physics*, 21, 7597–7609. Available from: https://acp.copernicus.org/articles/21/7597/2021/

Quimbayo-Duarte, J., Staquet, C., Chemel, C. & Arduini, G. (2019) Dispersion of tracers in the stable atmosphere of a valley opening onto a plain. *Boundary-Layer Meteorology*, 172, 291–315. Available from: https://doi.org/10.1007/s10546-019-00439-2

Sandradewi, J., Prévôt, A.S.H., Szidat, S., Perron, N., Alfarra, M.R., Lanz, V.A. et al. (2008) Using aerosol light absorption measurements for the quantitative determination of wood burning and traffic emission contributions to particulate matter. *Environmental Science & Technology*, 42, 3316–3323. Available from: https://doi.org/10.1021/es702253m

Sloane, C.S. (1984) Meteorologically adjusted air quality trends: visibility. *Atmospheric Environment (1967)*, 18, 1217–1229. Available from: https://doi.org/10.1016/0004-6981

Sokhi, R.S., Singh, V., Querol, X., Finardi, S., Targino, A.C., de Fatima Andrade, M. et al. (2021) A global observational analysis to understand changes in air quality during exceptionally low anthropogenic emission conditions. *Environment International*, 157, 106818. Available from: https://doi.org/10.5194/acp-2021-581-ac1

Solberg, S., Walker, S.-E., Schneider, P. & Guerreiro, C. (2021) Quantifying the impact of the Covid-19 lockdown measures on nitrogen dioxide levels throughout Europe. *Atmosphere*, 12, 131. Available from: https://doi.org/10.3390/atmos12020131

Song, Y.-Y. & Ying, L. (2015) Decision tree methods: applications for classification and prediction. *Shanghai Archives of Psychiatry*, 27, 13-0135. Available from: https://doi.org/10.11919/j.issn.1002-0829.215044

Stabile, L., Buonanno, G., Avino, P., Frattolillo, A. & Guerriero, E. (2018) Indoor exposure to particles emitted by biomass-burning heating systems and evaluation of dose and lung cancer risk received by population. *Environmental Pollution*, 235, 65–73. Available from: https://doi.org/10.1016/j.envpol.2017.12.055

Urgnani, R., Finco, A., Chiesa, M., Marzuoli, R., Bignotti, L., Riccio, A. et al. (2022) Size-segregated aerosol fluxes, deposition velocities, and chemical composition in an alpine valley. *Atmospheric Research*, 268, 105995. Available from: https://www.sciencedirect.com/science/article/pii/S0169809521005512

Vu, T.V., Shi, Z., Cheng, J., Zhang, Q., He, K., Wang, S. et al. (2019) Assessing the impact of clean air action on air quality trends in Beijing using a machine learning technique. *Atmospheric Chemistry and Physics*, 19, 11303–11314. Available from: https://doi.org/10.5194/acp-19-11303-2019

Walker, H.L., Heal, M.R., Braban, C.F., Ritchie, S., Conolly, C., Sanocka, A. et al. (2019) Changing supersites: assessing the impact of the southern UK EMEP supersite relocation on measured atmospheric composition. *Environmental Research Communications*, 1, 041001. Available from: https://doi.org/10.1088/2515-7620/ab1a6f

Whiteman, C.D. & Doran, J.C. (1993) The relationship between overlying synoptic-scale flows and winds within a valley. *Journal of Applied Meteorology*, 32, 1906–1912. Available from: https://doi.org/10.1175/1520-0450(1993)032%3C1669:TRBOSS%3E2.0.CO;2

Wong, J.P.S., Nenes, A. & Weber, R.J. (2017) Changes in light absorptivity of molecular weight separated Brown carbon due to photolytic aging. *Environmental Science & Technology*, 51, 8414–8421. Available from: https://doi.org/10.1021/acs.est.7b01739

Yan, J., Wang, X., Gong, P., Wang, C. & Cong, Z. (2018) Review of brown carbon aerosols: recent progress and perspectives. *Science of the Total Environment*, 634, 1475–1485. Available from: https://doi.org/10.1016/j.scitotenv.2018.04.083

Zardi, D. & Whiteman, C.D. (2013) Diurnal Mountain wind systems. In: *Springer atmospheric sciences*. Netherlands. URL:: Springer, pp. 35–119. Available from: https://doi.org/10.1007/978-94-007-4098-3_2

Ziegler, A. & König, I.R. (2014) Mining data with random forests: current options for real-world applications. *Wiley Interdisciplinary Reviews: Data Mining and Knowledge Discovery*, 4, 55–63. Available from: https://doi.org/10.1002/widm.1114

SUPPORTING INFORMATION

Additional supporting information can be found online in the Supporting Information section at the end of this article.

How to cite this article: Bertazza, E., Bisignano, A., Falocchi, M., & Giovannini, L. (2023). Effects of COVID-19 lockdown measures on nitrogen dioxide and black carbon concentrations close to a major Italian motorway. *Meteorological Applications*, *30*(2), e2123. https://doi.org/10.1002/met.2123